Design and Evaluation of a Fuzzy Assist Torque Map for Electric Power Steering Systems

1st Asal Khaleghi
Mechanical Engineering Department, Center of Advanced Rehabilitation and Robotics Research (FUM-CARE) Ferdowsi University of Mashhad
Mashhad, Iran
Asalkhaleghi@mail.um.ac.ir

2nd Mohammadreza Ghourchi
Electrical Engineering Department, Center of Advanced Rehabilitation and Robotics Research (FUM-CARE) Ferdowsi University of Mashhad
Mashhad, Iran
Mo.rezaghourchi@mail.um.ac.ir

3rd Ali Saadatpour
Electrical Engineering Department, Center of Advanced Rehabilitation and Robotics Research (FUM-CARE) Ferdowsi University of Mashhad
Mashhad, Iran
Ali.saadatpour@mail.um.ac.ir

4th Iman Kardan
Mechanical Engineering Department, Center of Advanced Rehabilitation and Robotics Research (FUM-CARE) Ferdowsi University of Mashhad
Mashhad, Iran
Iman.kardan@um.ac.ir

5th Mohammad-R Akbarzadeh-T
Electrical Engineering Department, Center of Excellence on Soft Computing and Intelligent Information Processing Ferdowsi University of Mashhad
Mashhad, Iran
Akbazar@um.ac.ir

6th Alireza Akbarzadeh
Mechanical Engineering Department, Center of Advanced Rehabilitation and Robotics Research (FUM-CARE) Ferdowsi University of Mashhad
Mashhad, Iran
Ali_akbarzadeh@um.ac.ir

Abstract*— This paper presents an integrated Electric Power Steering (EPS) framework that combines a two-degree-of-freedom lateral-yaw vehicle model, a detailed steering-column representation incorporating nonlinear friction and road-torque feedback, and a future-predictive driver steering model. To replace conventional saturated linear assist curves, a compact Sugeno-type fuzzy assist-torque map is developed as a nonlinear and computationally efficient alternative. Using a minimal rule base with Gaussian membership functions, the proposed map ensures smooth, continuous transitions across driver-torque and vehicle-speed inputs while avoiding the discontinuities inherent to piecewise linear formulations. System performance is assessed in a representative driving scenario with realistic road curvature, steering column disturbances, and operating conditions spanning both low-speed maneuvering and higher-speed stability regimes. Simulation results demonstrate that the proposed fuzzy assist strategy reduces driver workload when additional support is required yet intentionally restrains torque amplification at higher speeds to preserve stability and driver authority. Compared with the conventional saturated linear assist curve, the proposed approach also provides smoother steering-column responses, improved disturbance rejection, and lower motor-energy consumption, demonstrating its suitability for real-time EPS applications.

Keywords— Electric power steering, Steering assist, Assist characteristic, Assist curve, Fuzzy assist torque map, Future prediction steering control, Path tracking

I. INTRODUCTION

Power-assisted steering systems have become indispensable in modern vehicles, primarily due to increasing front-axle loads and the demand for agile, responsive steering behavior. The continuous rise in vehicle mass driven by enhanced passive safety requirements, added comfort and convenience systems, and expanded interior space has further elevated the steering torque required at the front wheels. To maintain steering effort within ergonomically acceptable limits, auxiliary power assistance has been introduced, transforming what was once a luxury feature into a standard system across nearly all passenger vehicles. Except for a few sub-compact models, such systems are now standard or optional in almost all passenger cars. Building on the foundation of manual steering, power steering retains the mechanical linkage between the steering wheel and the road wheels while introducing auxiliary torque through hydraulic, electro-hydraulic, or electric means. Conventional hydraulic power steering has long dominated the market, offering effective self-damping and isolation from road disturbances, but at the cost of continuous power draw and efficiency losses. The advent of electro-hydraulic systems addressed part of this issue by employing electronically controlled pumps that adjust flow in response to demand, thereby reducing energy consumption. More recently, the shift toward Electric Power Steering (EPS) has eliminated hydraulic components, utilizing an electric motor and control electronics to generate assistive torque directly. This transition not only reduces system weight and energy consumption but also enhances design flexibility and allows precise control of steering characteristics through software, paving the way for integration with advanced driver-assistance and automated driving systems [1], [2].

Following the widespread adoption of EPS, as its control architecture primarily determines performance, recent research has focused on developing algorithms capable of accurately modulating assist torque, adapting to vehicle dynamics, and maintaining both stability and a realistic steering feel across diverse operating conditions. In [3], a proportional-integral-derivative (PID) controller for an EPS system is implemented, achieving precise tracking and a fast transient response in the EPS's linear range; however, it is ineffective for the EPS's nonlinear characteristics [3]. A multi-map EPS control strategy based on changes in steering resistance torque under different front axle loads and adhesion coefficients is proposed in [4] to address excessive assist torque under low front axle loads and low adhesion coefficients. In [5], a Type-2 fuzzy logic controller is proposed for EPS motor torque control to improve assist performance across different vehicle speeds. However, the study's evaluation is limited to sinusoidal torque signals of varying frequencies, which may not fully capture the system behavior under realistic driving conditions. [6] proposed a non-linear robust control approach combining Sliding Mode Control (SMC) and Nonlinear Active Disturbance Rejection Control (NADRC) techniques. However, the authors noted that residual steady-state error in the steering motor current remains a key limitation, potentially affecting precise assist torque tracking and steering performance. In [7], a robust Linear Quadratic Regulator (LQR) for the EPS system is developed, where a Linear Quadratic Gaussian (LQG) compensator was employed to generate the control inputs for the LQR controller. In [8], a fuzzy-logic-based robust control framework was developed for EPS angle-tracking in an under-actuated system, specifically employing a two-layer structure to optimize both performance and disturbance attenuation.

Furthermore, consideration of road disturbances, particularly road reaction torque, is critical, as these factors fundamentally influence the driver's perception of steering feel and vehicle handling. An effective EPS control architecture must therefore achieve a delicate balance between attenuating undesirable road disturbances to enhance comfort and preserving essential feedback cues necessary for maintaining a natural and responsive steering sensation. The road reaction torque between the tires and road surface is transmitted from the front tires and tie rods to the rack bar; thus, a robust rack force estimation strategy is crucial. Various methods exist for estimating rack force. In [9], a model-reference control strategy was developed to actively reproduce desirable steering feel characteristics by overlaying a controlled feedback torque. In [10], the rack force was estimated using a nonlinear observer based on second-order steering system dynamics and steering sensor data, enabling accurate reconstruction of tire-road interaction forces to improve steering transparency and driver feedback. [11] proposed a road torque modeling method by using the LuGre tire model in the stationary and driving states and verified through experiment.

In the present work, the road-reaction torque was modeled by capturing the tire's self-aligning behavior and its transmission through the steering mechanism. The self-aligning moment was computed as a function of lateral tire force and pneumatic trail, reflecting the restoring moment generated by tire deformation during cornering. This moment was then converted to a steering-rack force and subsequently mapped to the steering column through the rack-and-pinion geometry. The resulting torque contributes directly to the driver- and motor-felt load at the steering wheel. By incorporating this mathematically derived road-reaction torque into the steering model, the simulation accurately reproduces the realistic feedback from tire–road interaction during lateral maneuvers.

The performance quality of electric power steering (EPS) systems is fundamentally determined by the assist-torque characteristic, which defines how the system relates driver torque and vehicle speed to the resulting assist torque. This characteristic directly influences steering feel, maneuverability, vehicle stability, and overall driver comfort, and it must therefore be shaped with great precision. The saturated linear characteristic curves are simple and meet the basic requirements for vehicle stability during motion. Conventional saturated linear assist curves are widely used in EPS research due to their simplicity and their ability to satisfy basic stability requirements during vehicle operation. Consequently, they appear extensively in the literature [12-20]. However, these mappings suffer from limited smoothness, particularly during transition phases. To mitigate this issue, [21] introduced a hybrid curve that blends linear and nonlinear behavior through a concave quadratic segment, offering only modest improvement in transition continuity. Another linear–nonlinear combination was explored in [22], arguing for a rapid assist increase at low speeds followed by a gradual reduction at higher speeds. A further mixed design was proposed in [23], applying nonlinear shaping at low speeds (below 20 km/h) and reverting to saturated linear behavior at higher speeds. Although this formulation improves the transition into the intermediate region, the shift into the saturated zone remains abrupt.

To address these limitations, the present work develops a unified EPS modeling and assist-map design framework grounded in fuzzy-logic methodology. Fuzzy logic offers two key properties particularly well suited to EPS assist-curve design: its universal approximation capability and its ability to incorporate qualitative expert knowledge directly into the mapping. As a nonlinear approximation tool, fuzzy logic can capture the complex relationship between driver torque, vehicle speed, and desired assist torque without imposing restrictive functional assumptions, thereby avoiding the limitations of polynomial or fixed-structure parametric curves. At the same time, the use of linguistically meaningful membership functions and rule bases preserves interpretability. It enables designers to encode steering-feel insights, such as assist suppression near zero torque or speed-dependent reduction of assist, directly into the controller.

The methodology introduced in this work integrates the proposed fuzzy-assist design with a mathematically derived steering-vehicle dynamic framework. This framework combines a two-degree-of-freedom lateral–yaw vehicle model with a high-fidelity steering column representation that incorporates torsion-bar elasticity, damping, inertia, and a fully modeled road-reaction torque term. The latter includes the tire self-aligning torque and its transmission through the steering mechanism, ensuring that the influence of road forces is accurately captured within the EPS dynamics. This integrated structure provides a realistic platform for evaluating the nonlinear fuzzy assist-torque map under representative steering conditions. A future-prediction driver steering model is incorporated to generate realistic human-like steering inputs and to provide a consistent closed-loop evaluation environment for all assist strategies considered. The assist-torque characteristic is realized through a Sugeno-type fuzzy inference structure defined over driver-torque and vehicle-speed domains. To maintain compactness, the rule base exploits the intrinsic symmetry of steering dynamics by applying mirrored rules for positive and negative torque regions, thereby reducing the total number of rules while preserving mapping accuracy and ensuring a fully symmetric assist characteristic.

This paper is structured as follows. Section II develops the mathematical models of vehicle dynamics and the electric power steering system. Section III introduces the future-prediction-based driver model used to generate steering-torque commands. Section IV describes the formulation of the fuzzy assist map. Section V outlines the overall simulation framework and test scenarios. Section VI presents the simulation results and provides a detailed discussion of the observed system behavior. Section VII concludes the paper with final remarks.

II. Mathematical Modeling of the Vehicle and EPS System

This section develops the complete mathematical model of vehicle lateral dynamics and the Electric Power Steering (EPS) mechanism. The model aims to capture the coupled interactions among the driver, steering system, and vehicle response, which form the foundation for assist-control design.
The overall system consists of two main subsystems:

1. The vehicle subsystem, describing the lateral and yaw dynamics using the 2-DOF bicycle model.

2. The steering subsystem consisting of the steering wheel, torsion bar, column/rack, and assist motor.

The integration of these subsystems results in an eight-state dynamic model that accurately represents the mechanical and kinematic coupling between the driver torque, assist motor torque, and the steering-induced tire forces.
The vehicle dynamics are represented using a 2-DOF lateral-yaw bicycle model coupled with a second-order steering system model. This control-oriented modeling framework was selected because it captures the dominant vehicle responses directly influencing EPS performance, namely lateral motion, yaw motion, steering-column dynamics, and driver–vehicle interaction. The 2-DOF bicycle model remains one of the most widely adopted models for steering control and path-tracking applications due to its ability to accurately represent the essential lateral vehicle dynamics while maintaining computational efficiency. Furthermore, the use of simplified lateral-yaw models is common in controller design, real-time implementation, and hardware-in-the-loop applications, where an appropriate balance between model fidelity and computational complexity is required. Therefore, the adopted model is well suited for the investigation of steering assistance characteristics and driver torque reduction addressed in this study.

A. *Vehicle lateral-yaw dynamics*

The vehicle dynamics are modeled using a two-degree-of-freedom single-track (bicycle) representation, as illustrated in Fig. 1, adopted from [24], which captures the vehicle's essential lateral and yaw motions while assuming constant forward velocity. The lateral velocity *v* is measured at the vehicle's center of mass, and the yaw rate, $\dot{\psi}$ defines the rotational motion about the vehicle's vertical axis. The yaw angle ψ specifies the vehicle's orientation relative to the global x-axis, while the steering input δ acts on the front tires to generate lateral forces. Effects such as roll and pitch are disregarded to maintain a planar motion model that remains accurate for typical steering maneuvers.

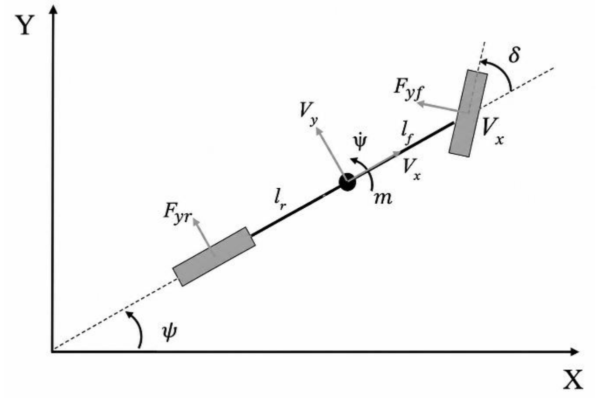

Fig. 1 2 DOF vehicle model [24]

The governing dynamic equations are expressed as:

$$m(\ddot{y} + V_x\dot{\psi}) = F_{yf} + F_{yr} \quad (1)$$

$$I_z\ddot{\psi} = l_f F_{yf} - l_r F_{yr} \quad (2)$$

Here, y denotes the lateral displacement of the vehicle's center of gravity (CG), V_y is the lateral velocity, ψ is the yaw angle, and $\dot{\psi}$ and $\ddot{\psi}$ are the yaw rate and the yaw acceleration. The constant V_x is the longitudinal velocity, and m and I_z are the vehicle mass and yaw inertia, respectively. l_f and l_r are the longitudinal distances from the center of mass to the front and rear axles. The tire lateral forces F_{yf} and F_{yr} referring to front tires and rear tires, respectively, are assumed to be proportional to tire slip angles α_f and α_r. Therefore, expressed as:

$$F_{yf} = 2C_{\alpha f}\left(\delta - \frac{V_y + l_f\dot{\psi}}{V_x}\right) \quad (3)$$

$$F_{yr} = 2C_{\alpha r}\left(-\frac{V_y - l_r\dot{\psi}}{V_x}\right) \quad (4)$$

The parameters $C_{\alpha f}$ and $C_{\alpha r}$ represent the linear cornering stiffness of the front and rear tires.
The state space equations of the vehicle model are represented as:

$$\begin{bmatrix}\dot{y}\\ \dot{V}_y\\ \dot{\psi}\\ \ddot{\psi}\end{bmatrix} = \begin{bmatrix}0 & 1 & V_x & 0\\ 0 & -\frac{2C_{\alpha f}+2C_{\alpha r}}{mV_x} & 0 & V_x - \frac{2C_{\alpha f}l_f-2C_{\alpha r}l_r}{mV_x}\\ 0 & 0 & 0 & 1\\ 0 & -\frac{2C_{\alpha f}l_f-2C_{\alpha r}l_r}{I_zV_x} & 0 & -\frac{2C_{\alpha f}l_f^2+2C_{\alpha r}l_r^2}{I_zV_x}\end{bmatrix}\begin{bmatrix}y\\ V_y\\ \psi\\ \dot{\psi}\end{bmatrix} + \begin{bmatrix}0\\ \frac{2C_{\alpha f}}{m}\\ 0\\ \frac{2C_{\alpha f}l_f}{I_z}\end{bmatrix}\delta \quad (5)$$

For the simulations presented in this work, the longitudinal velocity was specified as a constant value for each driving scenario. This assumption is commonly employed in linear bicycle-model formulations and enables the lateral-yaw dynamics to be analyzed under well-defined operating conditions. Previous studies have similarly adopted a constant longitudinal velocity when developing path-tracking and steering controllers based on the bicycle model.

In practical driving situations involving simultaneous steering and significant acceleration or braking, the longitudinal velocity becomes time-varying, which may introduce additional coupling between longitudinal and lateral vehicle dynamics. Variations in longitudinal speed influence tire slip angles and lateral force generation, thereby affecting the transient steering response. Nevertheless, for the path-following maneuvers and operating conditions considered in this study, the constant-velocity assumption provides a suitable representation for evaluating EPS assistance performance while preserving model simplicity and computational efficiency. Future work may incorporate a coupled longitudinal-lateral vehicle model to investigate EPS behavior under combined steering, braking, and acceleration maneuvers.

B. *EPS system dynamics*

The Electric Power Steering (EPS) subsystem, as illustrated in Fig. 2, adopted from [24], is formulated as a mechanically coupled system that transmits torque from the driver to the steering rack through a compliant torsion bar. It consists of the steering wheel**,** torsion bar**,** steering column and rack, and the assist motor, with the road reaction torque providing feedback from the tires to the driver.

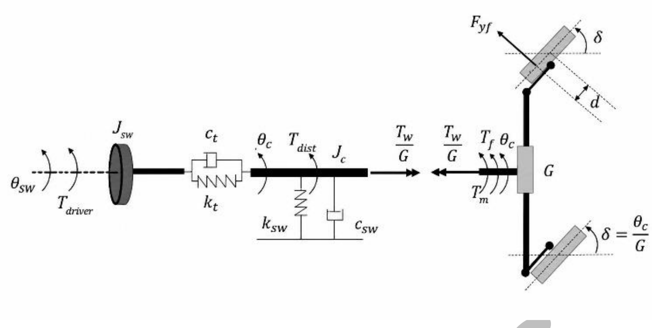

Fig. 2 Steering system model integrated with the vehicle model [24]

The steering wheel and torsion bar dynamics are modeled as a second-order rotational system:

$$J_{sw}\ddot{\theta}_{sw} = T_{driver} - k_t(\theta_{sw} - \theta_c) - c_t(\dot{\theta}_{sw} - \dot{\theta}_c) \quad (6)$$

Where $\theta_{sw}, \dot{\theta}_{sw}$ *and* $\ddot{\theta}_{sw}$ are steering wheel angle, angular velocity and angular acceleration respectively. J_{sw} is the steering wheel inertia, k_t and c_t are the torsion bar stiffness and damping, and T_{driver} is the torque applied by the driver. The term $(\theta_{sw} - \theta_c)$ represents the torsional twist of the bar, which is proportional to the driver's applied torque and is commonly used as the EPS torque sensor signal.

The steering column and rack dynamics are expressed as:

$$J_c\ddot{\theta}_c = c_t(\dot{\theta}_{sw} - \dot{\theta}_c) + k_t(\theta_{sw} - \theta_c) - c_{sw}\dot{\theta}_c - k_{sw}\theta_c + T_m - T_f - T_{dist} - \frac{T_w}{G} \quad (7)$$

where $\theta_c, \dot{\theta}_c$ *and* $\ddot{\theta}_c$ denote the steering-column angle, angular velocity, and angular acceleration, respectively, J_c is the equivalent column/rack inertia, k_{sw} and c_{sw} represent structural stiffness and damping, T_m is the assist motor torque, and T_{dist} is the disturbance torque from road inputs. The term T_w denotes the wheel-side aligning torque caused by tire lateral forces, given by:

$$T_w = F_{yf}d \quad (8)$$

Where d denotes both the pneumatic trail and mechanical trail of the front tires combined, which is a property of the tire. The inclusion of the self-aligning torque T_w ensures that the steering column dynamics are directly influenced by road feedback, allowing tire-generated aligning moments arising from lateral force and pneumatic trail to propagate back through the rack into the steering wheel. This feedback is essential for producing a realistic on-center feel, natural self-centering behavior, and accurate assessment of how assist algorithms interact with genuine road-induced moments.

The term T_f denotes the equivalent friction torque acting on the steering mechanism. Following the nonlinear friction modeling approach presented in [25], the friction torque is modeled as the combination of a viscous component and a nonlinear Coulomb component,

$$T_f = c_v\dot{\theta}_c + \tau_f \tanh(k_f\dot{\theta}_c) \quad (9)$$

where c_v is the equivalent viscous friction coefficient, τ_f is the Coulomb friction torque, k_f is the transition coefficient. The viscous term represents speed-dependent energy dissipation arising from bearings, lubrication, and other mechanical losses, while the nonlinear term models dry friction in the steering mechanism. The hyperbolic tangent provides a smooth approximation of the discontinuous sign function, improving numerical stability while accurately capturing the nonlinear friction characteristics near zero velocity. The friction torque acts in opposition to the steering-column motion and is incorporated into the steering-column dynamics, resulting in a nonlinear state-space representation.

The steering ratio G, transforms the steering column angle to the front tires' steering angle as,

$$\delta = \frac{\theta_c}{G} \tag{10}$$

The complete EPS-vehicle system is represented in the state-space in the form of:

$$\begin{cases} \dot{x} = Ax + Bu + f(x) \\ y = x \end{cases} \tag{11}$$

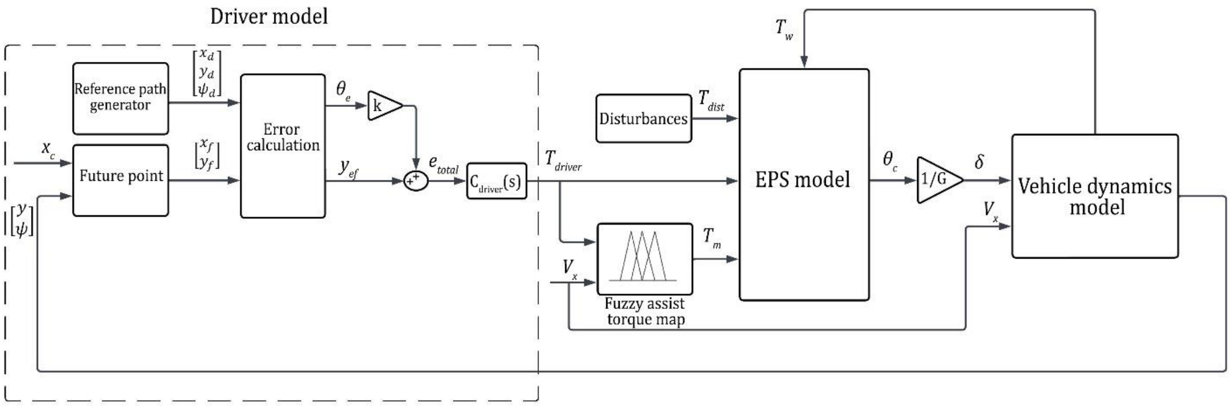

Fig. 3 Proposed control system

Where $x = [y \quad V_y \quad \psi \quad \dot{\psi} \quad \theta_{sw} \quad \dot{\theta}_{sw} \quad \theta_c \quad \dot{\theta}_c]^T$ is the state vector, and $u = [T_{dist} \quad T_{driver} \quad T_m]^T$ is the input vector, f(x) represents the nonlinear friction term introduced to account for the equivalent mechanical friction of the steering mechanism. and the output vector is $y = x$.

Therefore, the state-space equations of the EPS-Vehicle are:

$$\begin{bmatrix} \dot{y} \\ \dot{V}_y \\ \dot{\psi} \\ \ddot{\psi} \\ \dot{\theta}_{sw} \\ \ddot{\theta}_{sw} \\ \dot{\theta}_c \\ \ddot{\theta}_c \end{bmatrix} = \begin{bmatrix} 0 & 1 & V_x & 0 & 0 & 0 & 0 & 0 \\ 0 & a_{22} & 0 & a_{24} & 0 & 0 & a_{27} & 0 \\ 0 & 0 & 0 & 1 & 0 & 0 & 0 & 0 \\ 0 & a_{42} & 0 & a_{44} & 0 & 0 & a_{47} & 0 \\ 0 & 0 & 0 & 0 & 0 & 1 & 0 & 0 \\ 0 & 0 & 0 & 0 & a_{65} & a_{66} & a_{67} & a_{68} \\ 0 & 0 & 0 & 0 & 0 & 0 & 0 & 1 \\ 0 & a_{82} & 0 & a_{84} & a_{85} & a_{86} & a_{87} & a_{88} \end{bmatrix} \begin{bmatrix} y \\ V_y \\ \psi \\ \dot{\psi} \\ \theta_{sw} \\ \dot{\theta}_{sw} \\ \theta_c \\ \dot{\theta}_c \end{bmatrix} + \begin{bmatrix} 0 & 0 & 0 \\ 0 & 0 & 0 \\ 0 & 0 & 0 \\ 0 & 0 & 0 \\ 0 & 0 & 0 \\ 0 & \frac{1}{J_{sw}} & 0 \\ 0 & 0 & 0 \\ -\frac{1}{J_c} & 0 & \frac{1}{J_c} \end{bmatrix} \begin{bmatrix} T_{dist} \\ T_{driver} \\ T_m \end{bmatrix} + \begin{bmatrix} 0 \\ 0 \\ 0 \\ 0 \\ 0 \\ 0 \\ 0 \\ -\frac{\tau_f \tanh(\dot{\theta}_c)}{J_c} \end{bmatrix} \tag{12}$$

where $a_{22} = -\frac{2C_{\alpha f}+2C_{\alpha r}}{mV_x}$, $a_{24} = V_x - \frac{2C_{\alpha f}l_f - 2C_{\alpha r}l_r}{mV_x}$, $a_{27} = \frac{2C_{\alpha f}}{mG}$, $a_{42} = -\frac{2C_{\alpha f}l_f - 2C_{\alpha r}l_r}{I_z V_x}$, $a_{44} = -\frac{2C_{\alpha f}l_f^2 + 2C_{\alpha r}l_r^2}{I_z V_x}$, $a_{47} = \frac{2C_{\alpha f}l_f}{I_z G}$, $a_{65} = -\frac{k_t}{J_{sw}}$, $a_{66} = -\frac{c_t}{J_{sw}}$, $a_{67} = \frac{k_t}{J_{sw}}$, $a_{68} = \frac{c_t}{J_{sw}}$, $a_{82} = \frac{2C_{\alpha f}d}{GV_xJ_c}$, $a_{84} = \frac{2C_{\alpha f}l_f d}{GV_xJ_c}$, $a_{85} = \frac{k_t}{J_c}$, $a_{86} = \frac{c_t}{J_c}$, $a_{87} = -\left(\frac{k_t + k_{sw}}{J_c} + \frac{2C_{\alpha f}d}{G^2 J_c}\right)$, $a_{88} = -\frac{c_t + c_{sw} + c_v}{J_c}$

Table I details the specific parameters used for the vehicle and EPS models.

TABLE I. MATHEMATICAL MODEL PARAMETERS

Abbr.	Model Parameter	Value	Unit
$\boldsymbol{m}$	Mass of the vehicle	1380	kg
$\boldsymbol{I_z}$	Yaw moment of inertia	0.25	$kg.m^2$
$\boldsymbol{l_f}$	Distance from COM to front tires	0.98	m
$\boldsymbol{l_r}$	Distance from COM to rear tires	1.49	m
$\boldsymbol{C_{\alpha f}}$	Lateral front tire stiffness	49750	N/rad
$\boldsymbol{C_{\alpha r}}$	Lateral rear tires stiffness	49750	N/rad
$\boldsymbol{J_{sw}}$	Inertia of the steering wheel	0.0216	$kg.m^2$
$\boldsymbol{k_{sw}}$	Stiffness of the steering system due to the kingpin axes (inclination and scrub radius)	0.516	Nm/rad
$\boldsymbol{c_{sw}}$	Damping coefficient of the steering system (of the bearings) and steering system friction	0.2	Nms/rad
$\boldsymbol{J_c}$	Inertia of the rack and the front wheels referred to the pinion	0.01	$kg.m^2$
$\boldsymbol{k_t}$	Stiffness coefficient of the torsion bar	115	Nm/rad
$\boldsymbol{c_t}$	Damping coefficient of the torsion bar	1.74	Nms/rad
$\boldsymbol{d}$	Trail (Pneumatic and caster)	0.059	m
$\boldsymbol{G}$	Steering gear ratio	16	-
$\boldsymbol{c_v}$	Equivalent viscous friction coefficient	0.2	Nms/rad
$\boldsymbol{\tau_f}$	Coulomb friction torque	0.4	$N.m$
$\boldsymbol{k_f}$	Transition coefficient	5	-

III. INTELLIGENT DRIVER MODELING

In the proposed control framework illustrated in Fig. 3, a future-predictive driver model was developed to generate a realistic steering torque demand for the EPS system. In this approach, the driver's steering behavior is modeled using a future prediction method, building on the technique described in [26] and further modified to enhance its human-like steering response and predictive accuracy, making it suitable for this EPS system application. The driver uses both the current vehicle state and a future point along the reference path to calculate steering errors and determine the corrective torque.

The reference generator provides the desired longitudinal and lateral positions and the reference heading angle, denoted as $x_{\text{ref}}, y_{\text{ref}}, \psi_{\text{ref}}$. The current longitudinal and lateral positions of the vehicle's center of mass, denoted x_c and y_c, are obtained from the vehicle model, with x_c computed by integrating the longitudinal velocity,

$$x_c = \int V_x dt \tag{13}$$

while y_c and yaw angle ψ_c are taken directly from the vehicle model.

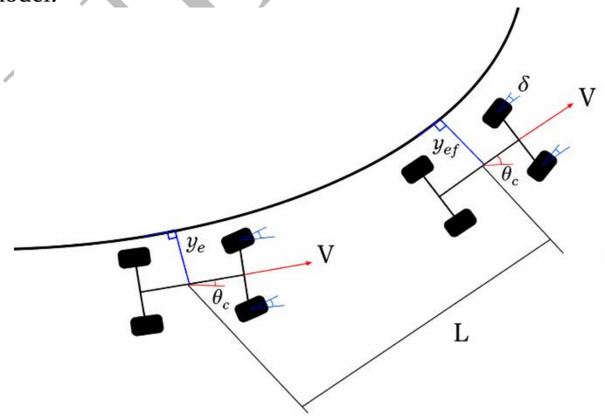

Fig. 4 preview points [26]

As illustrated in Fig. 4, to incorporate a forward-looking effect similar to human driving, a preview point is defined using a variable preview distance L as

$$x_f = L\cos\psi_c + x_c \tag{14}$$

$$y_f = L\sin\psi_c + y_c \tag{15}$$

Where x_f and y_f denote longitudinal and lateral positions, respectively. To ensure consistent prediction across varying speeds and curvatures, the prediction distance L is defined as,

$$L(v,\kappa) = sat\left(\frac{vT_p}{1+\gamma|\kappa|}, L_{min}, L_{max}\right) \tag{16}$$

where κ represents the instantaneous path curvature, v is the vehicle's longitudinal velocity, T_p is the nominal prediction time constant, γ is the curvature sensitivity coefficient, and L_{min}, L_{max} denote the saturation bounds. A first-order low-pass filter ensures smooth and stable variation of L. This formulation enables the driver model to shorten the prediction horizon in tight curves for improved path conformity and extend it in straight-line segments for better stability. Since curvature κ is computed directly from the path geometry, this approach can be applied to any arbitrary road trajectory and remains robust under all driving and path conditions. This preview mechanism allows the driver model to respond not only to current deviations but also to upcoming road curvature.

Two main error signals are computed: the heading error and the lateral error at the preview point.

The heading error is:

$$\psi_e = \psi_{\text{ref}} - \psi_c \tag{17}$$

The lateral error relative to the preview point is obtained by projecting the difference between the reference position and the preview position into the vehicle's body frame:

$$Y_{ef} = \cos(\psi_c)\,(y_{\text{ref}} - y_f) - \sin(\psi_c)\,(x_{\text{ref}} - x_f) \tag{18}$$

To form a single control input, a weighted combination of both errors is used:

$$e_{total} = y_{ef} + k\,\psi_e \tag{19}$$

where k is a tuning parameter that adjusts the influence of the heading error.

C. Driver Torque Generation

The combined error e_{total} is passed through a PID controller denoted as $C_d(s)$ as

$$C_d(s) = K_p + k_i\frac{1}{s} + K_d\frac{N}{1+N\frac{1}{s}} \tag{20}$$

which represents the neuromuscular response of the driver, generating torque commands in proportion to deviation,

$$T_{driver} = C_{driver}(s)e_{total} \tag{21}$$

The resultant T_d serves as the human steering input to the EPS-vehicle system.
The control parameters utilized in the driver model, obtained via an iterative simulation procedure, are provided in Table II.

TABLE II. CONTROL PARAMETERS OF THE DRIVER MODEL

Abbr.	Model Parameter	Value	Unit
$\mathbf{K_{p,d}}$	Proportional gain	8	N
$\mathbf{K_{i,d}}$	Integral gain	5	N/s
$\mathbf{K_{d,d}}$	Derivative gain	1	N.s
$\mathbf{N_d}$	Filter coefficient	100	-
$\boldsymbol{k}$	Angular error gain	15	m/rad
$\boldsymbol{T_p}$	Nominal Prediction time constant	0.144	s
$\boldsymbol{L_{min}}$	Prediction distance Lower bound	0.2	m
$\boldsymbol{L_{max}}$	Prediction distance upper bound	2	m
$\boldsymbol{\gamma}$	curvature sensitivity coefficient	5	-

IV. DESIGN OF THE FUZZY ASSIST TORQUE MAP

The assist-torque characteristic was designed using a fuzzy-logic framework. The system is constructed to achieve the desired mapping using the minimum number of rules while still satisfying the essential requirements of the assist curve. Increasing the number of rules, membership functions, or input partitions may increase modeling precision [27], yet it also complicates the structure and reduces transparency. Therefore, the design strategy emphasizes a compact, efficient rule base capable of achieving the desired nonlinear behavior while keeping the fuzzy system's computational load low and maintaining interpretability. To implement this strategy, a Sugeno-type fuzzy inference system is employed, as previously described in the literature, in which the consequent part of each rule is represented by either a constant value or a linear combination of the input variables.
This configuration ensures smoothness, numerical stability, and suitability for real-time control applications. To construct the desired nonlinear mapping, the input space is first partitioned using fuzzy membership functions. as illustrated in Fig. 5 The driver-torque domain is divided into three non-overlapping fuzzy sets with equal support, and the vehicle-speed domain is also partitioned into the conventional three-set structure representing low, medium, and high speeds. During refinement, as illustrated in Fig. 6, overlap was explicitly introduced to achieve smoother transitions and improved continuity, and the membership shapes were ultimately modified to Gaussian forms to achieve the desired behavior and smoother blending across operating regions.

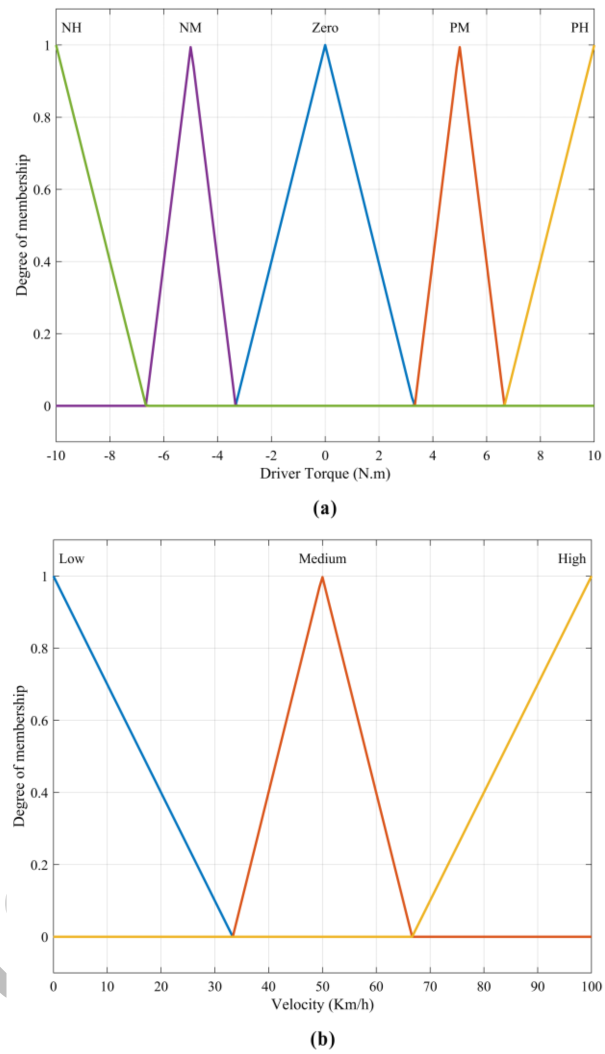

Fig. 5 Initial Fuzzy partitioning. (a) Driver torque partitioning (b) velocity partitioning

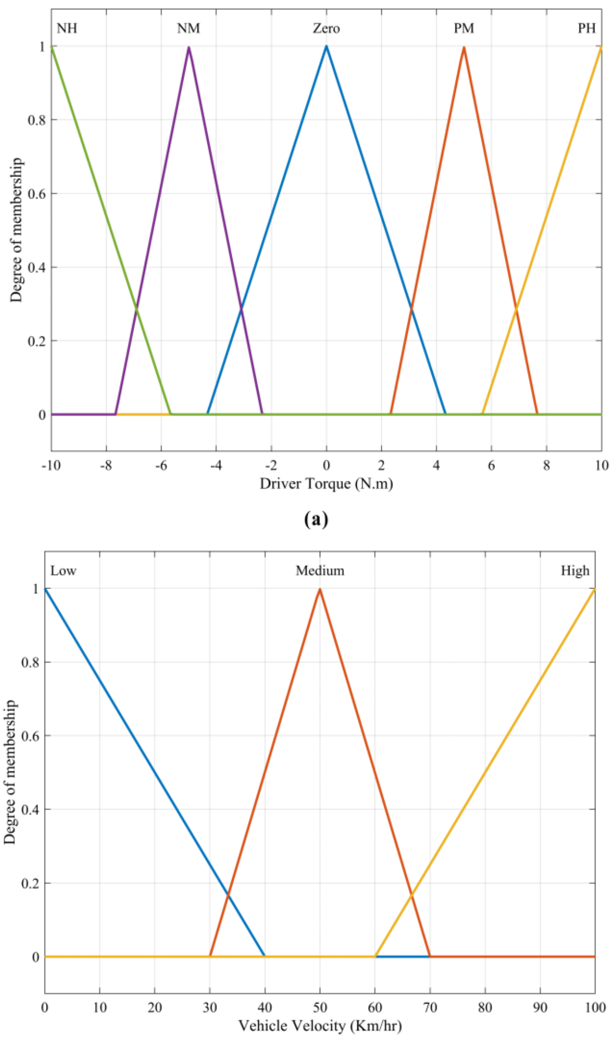

Fig. 6 Overlapped Fuzzy partitioning. (a) Driver torque partitioning (b) velocity partitioning

After achieving the desired results with overlapping triangular membership functions, Gaussian membership functions were used to enhance continuity and smoothness. As represented in Fig. 7 and Fig. 8.

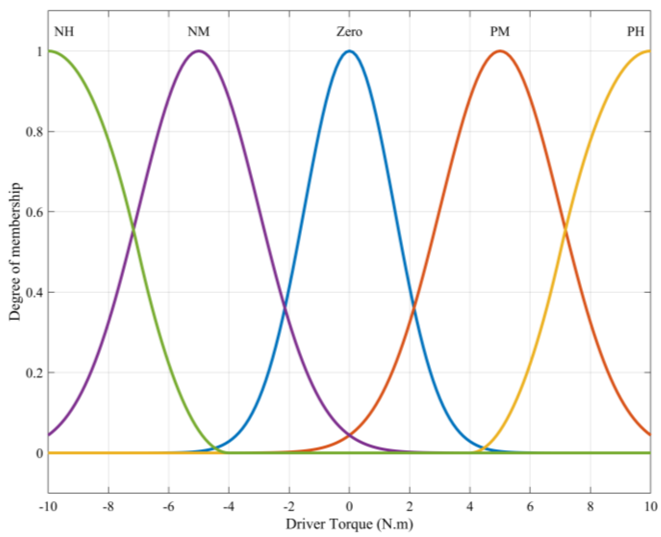

Fig. 7 Driver torque Gaussian membership function

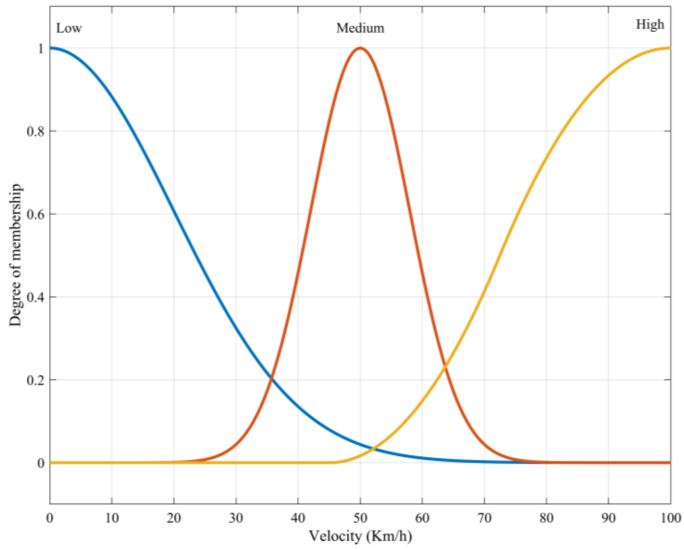

Fig. 8 Velocity Gaussian membership function

The rule set of the proposed Sugeno-type fuzzy system is detailed in Table III.

TABLE III. FUZZY SYSTEM RULE SET

Velocity	**Slow**	**Medium**	**High**
Driver Torque (T_{driver})		**Assist Torque**	
PH	12	8	4
PM	T_{driver}	$0.8T_{driver}$	$\mathbf{0.6}\boldsymbol{T_{driver}}$
Zero	0	0	0
NH	T_{driver}	$0.8T_{driver}$	$\mathbf{0.6}\boldsymbol{T_{driver}}$
NM	-12	-8	-4

Fig. 9 demonstrates the Fuzzy rule inference.

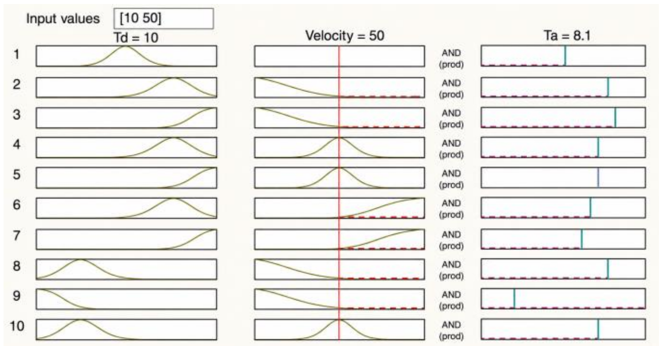

Fig. 9 Fuzzy rule inference

The control surface generated from the final rule base, as illustrated in Fig. 10, reflects the expected nonlinear behavior of the assist characteristic.

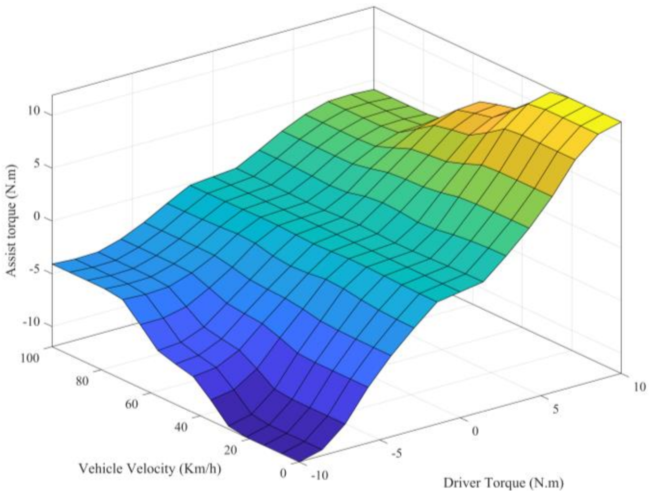

Fig. 10 Fuzzy control surface

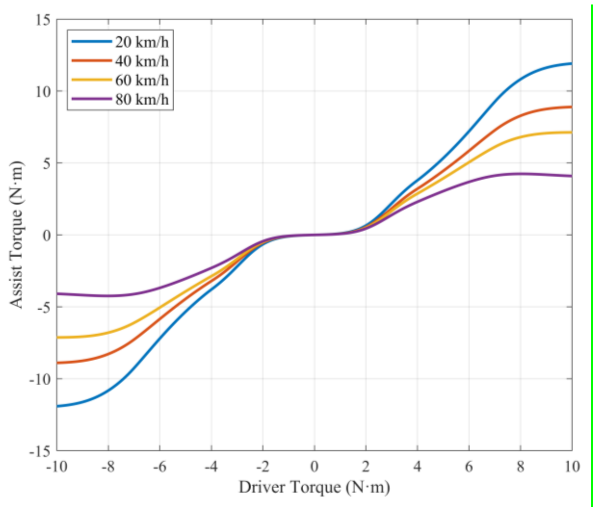

Fig. 11 Fuzzy assist torque map

Examination of the resulting control surface shows that the fuzzy-designed characteristic provides a smooth, continuous, and progressive increase in assist torque as the driver torque increases from zero, thereby improving precision in the low-torque region and eliminating the abrupt transitions common in crisp or segmented assist maps. This gradual response enhances steering feel and prevents discontinuities that can undermine the driver's confidence. The characteristic also demonstrates appropriate dependence on vehicle speed; the assist torque is intentionally reduced as speed increases, preserving road feedback, enhancing stability, and preventing excessive assistance at high-speed conditions. This speed-dependent reduction directly reduces energy consumption, since the EPS actuator demands less electrical power at operating points where high assist is neither necessary nor desirable. Moreover, smoother, more predictable torque transitions reduce unnecessary fluctuations in motor current, improving thermal performance and extending the operational life of the steering components. At very high speeds, the reduced assist allows the driver to retain stronger control authority. In contrast, at low speeds, the system still supplies sufficient support for maneuvering with minimal physical effort. To further illustrate the practical behavior of the proposed fuzzy assist torque map, Fig. 11 presents the resulting EPS assist characteristics, showing the motor assist torque as a function of the driver-applied steering torque for several representative vehicle speeds. The curves clearly demonstrate the desired nonlinear and speed-dependent assist behavior, providing higher motor assistance at low vehicle speeds to reduce steering effort while progressively decreasing the assist as vehicle speed increases, thereby preserving steering feel, road feedback, and vehicle stability.

V. SIMULATION FRAMEWORK

All simulations were performed in the MATLAB/Simulink environment. A driving path was designed using MATLAB's *Driving Scenario Designer* and exported as a MATLAB function to the Simulink model. This function provides the reference longitudinal and lateral positions, as well as the reference heading angle, at each simulation step.

This driving path is illustrated in Fig. 11. To ensure that the driver model performs reliably under a wide range of operating conditions, this path was intentionally constructed to include straight segments, smooth bends, and sections with relatively sharp curvature.

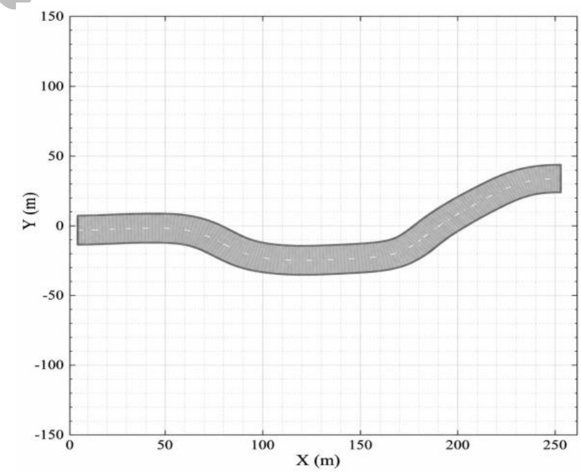

Fig. 12 Driving path constructed in MATLAB's *driving scenario designer*

This diversity allows the simulation to capture representative real-world driving scenarios, including lane keeping, moderate turning, and more demanding cornering maneuvers. By exposing the driver model to both mild and extreme curvature changes, the evaluation becomes more robust and ensures that the proposed control strategy behaves consistently across the full spectrum of steering tasks encountered in typical road environments.

Simulations were conducted for both reference paths under four distinct operating cases, designed to observe the behavior of the proposed control system and steering assist across both low and high speeds, and under external disturbance conditions.

Case I. *Low-Speed Operation:*

This case evaluates the system at a low, constant vehicle speed of 20 km/h to assess baseline performance and steering feel during low-speed maneuvers.

Case II. *High-Speed Operation:*

This case evaluates the system at a higher, constant speed of 50 km/h to observe system behavior and stability during typical high-speed driving. The comparison between Case I and Case II is critical for assessing speed-dependent performance steering assist.

Case III. *Low-Speed Disturbance-Rejection Test:*

A disturbance-rejection test is performed at a low speed of 20 km/h by applying an external disturbance torque to the steering column. The disturbance is modeled as a time-varying torque proportional to the road reaction torque, expressed as

$$T_{dist} = 0.125T_w + 0.025T_w \sin(2\pi f t) \quad (22)$$

where T_w is the road reaction torque and $f = 3\,Hz$. The constant component represents an equivalent external steering load corresponding to approximately 12.5% of the road reaction torque, while the sinusoidal component introduces a small periodic variation with an amplitude of 2.5% of T_w, simulating realistic fluctuations caused by road surface irregularities and steering-system disturbances. This formulation provides a deterministic and repeatable disturbance, enabling a consistent evaluation of the disturbance-rejection capability of the proposed EPS assist strategies.

Case IV. *High-Speed Disturbance-Rejection Test:*

This case repeats the disturbance-rejection test at a constant speed of 50 km/h using the same disturbance torque applied in Case III. The objective is to evaluate the effectiveness of the proposed assist strategies in attenuating external steering disturbances and maintaining stable steering performance under high-speed driving conditions.

To evaluate the performance of the proposed fuzzy assist map, simulations were performed alongside a benchmark assist strategy based on the saturated linear assist curve proposed in [19] which is illustrated in Fig. 12. The reference assist curve defines the motor assist torque T_M based on steering torque input and vehicle velocity as

$$T_M = \begin{cases} 0, & 0 \le T_d \le T_{d0} \\ trq(v), & T_{d0} \le T_d \le T_{dmax} \\ T_N, & T_{dmax} \le T_d \end{cases} \quad (23)$$

where the speed-dependent linear region is given by

$$trq(v) = (4 - 0.0606v + 0.0003v^2)(T_d - T_{d0}) \quad (24)$$

where $T_{d0} = 1\,N.m$ and $T_{dmax} = 7\,N.m$.

This saturation-type assist law serves as a conventional baseline against which the proposed fuzzy assist curve is compared in terms of steering behavior, driver torque demand, and disturbance handling across all simulation scenarios.

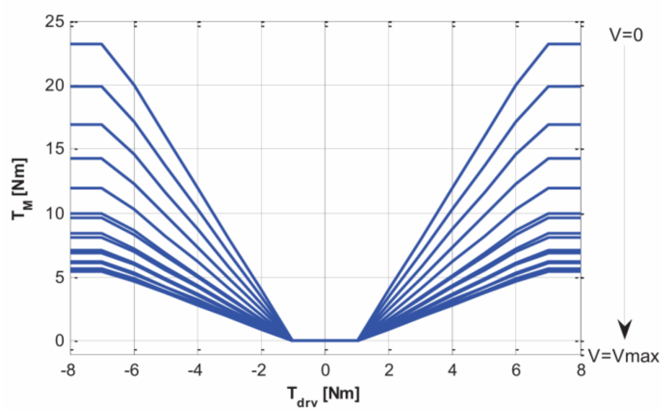

Fig. 13 Saturated linear assist curve proposed in [19]

VI. Simulation Results and Discussion

The simulations were carried out for the four operating cases defined earlier.

For each case, three configurations were evaluated:

1. Not Assisted (baseline)
2. Fuzzy Assist Map (proposed)
3. Saturated Linear Assist Curve (benchmark)

A comprehensive comparison was conducted using:

- path-tracking accuracy
- driver torque
- steering column angle
- steering column angular velocity
- disturbance response

- motor energy consumption

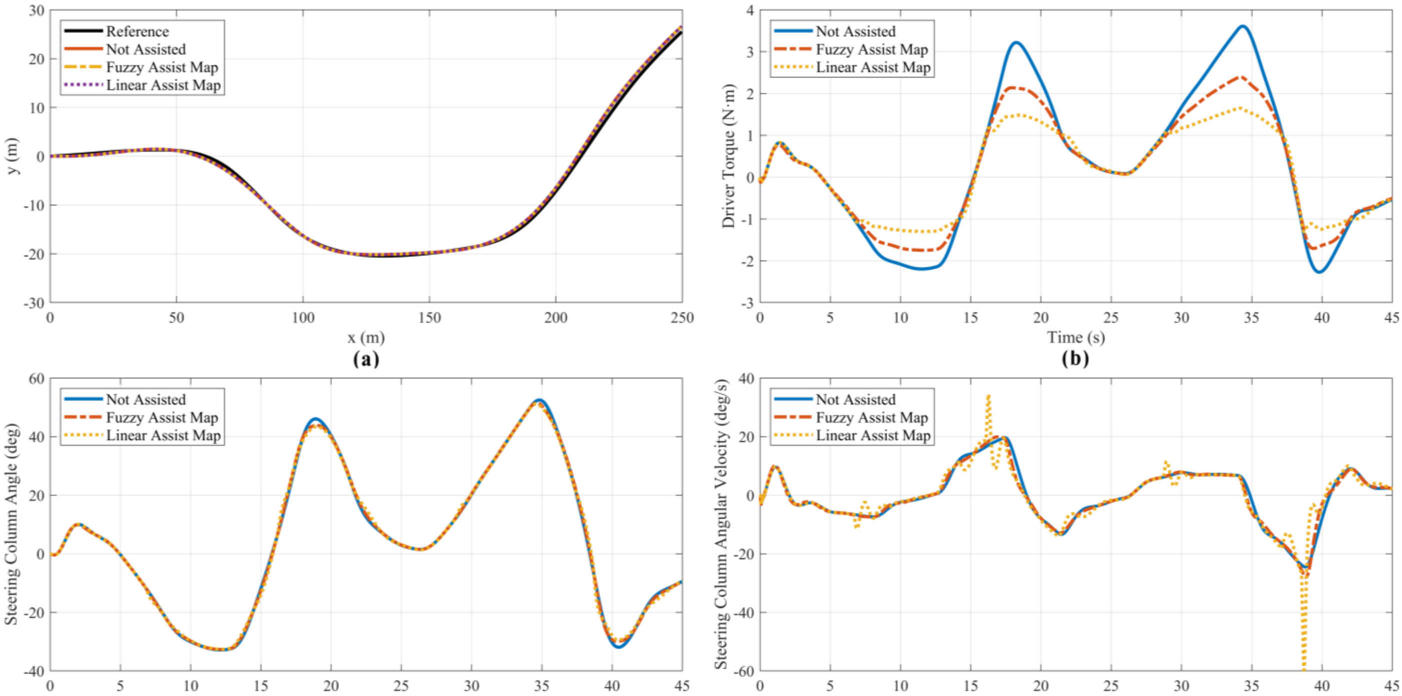

Fig. 14 ***(Case I. V=20 km/h)***. (a) path tracking performance (b) Driver torque demand (c) steering column angle (d) steering column angular velocity

Tracking accuracy is summarized in Tables IV and V, which report the maximum and RMS tracking errors for all cases and all assist strategies.

Motor energy consumption E_m was evaluated across all four simulation cases using the mechanical power relation. The total energy usage over the simulation horizon was then obtained through numerical integration as

$$\cancel{T_m(t) = \dot{\theta}_c(t)\, dt} \qquad \cancel{(25)}$$

$$E_m = \int |\, T_m(t)\ \dot{\theta}_c\, | dt \qquad (25)$$

where the absolute value was applied to ensure that both positive and negative steering work contributions are accumulated as physically consumed energy. This formulation represents the physical mechanical energy delivered by the EPS actuator to the steering rack, independent of electrical conversion effects, and therefore directly reflects how aggressively each assist strategy drives the steering system.

a) Case I. Low-Speed Operation (20 km/h)

The low-speed scenario evaluates the behavior of the assist strategies during a path-following maneuver under nominal operating conditions. As shown in Fig. 14(a), all three configurations accurately follow the reference trajectory, with only small deviations throughout the maneuver. Consistent with the results presented in Table IV, both assist strategies slightly improve the path-tracking performance relative to the unassisted case by reducing both the maximum and RMS tracking errors. These results indicate that although steering assistance provides a modest improvement in tracking accuracy, its primary contribution is the reduction of driver steering effort while preserving accurate path-following performance.

This improvement is clearly reflected in Fig. 14(b), where both assist strategies substantially reduce the driver torque throughout the maneuver. According to Table IV, the proposed fuzzy assist map reduces the maximum and RMS driver torque by 33.65% and 22.68%, respectively, while the saturated linear assist curve achieves larger reductions of 54.30% and 39.61%. The greater torque reduction achieved by the linear assist curve results from its higher assist gain, which provides assistance even under relatively small steering demands. Although this minimizes driver effort, it also increases the likelihood of unnecessary motor assistance. In contrast, the fuzzy assist map adapts the assist level according to the steering demand, providing sufficient assistance while avoiding excessive intervention.

The steering column angle responses shown in Fig. 14(c) remain very similar for all configurations, confirming that neither assist strategy alters the intended steering command or compromises the steering trajectory. More significant differences are observed in the steering column angular velocity response shown in Fig. 14(d). As quantified in Table VI, the saturated linear assist curve produces substantially larger transient angular-velocity deviations, reaching a maximum error of 35.32 deg/s, compared with only 5.69 deg/s for the proposed fuzzy assist map. Consequently, the linear assist curve exhibits abrupt changes in steering motion, whereas the fuzzy assist map maintains a considerably smoother and more continuous angular-velocity profile. This behavior indicates improved transient steering characteristics and a more natural steering feel while still providing a significant reduction in driver effort.

Overall, both assist strategies successfully reduce steering effort without compromising path-following performance. However, the proposed fuzzy assist map achieves a more balanced trade-off between driver torque reduction and steering smoothness, delivering effective assistance while avoiding the excessive steering dynamics introduced by the saturated linear assist curve.

b) Case II. High-Speed Operation (50 km/h)

The high-speed scenario evaluates the effectiveness of the assist strategies during the same path-following maneuver at an increased vehicle speed. As shown in Fig. 15(a), both assist strategies improve the vehicle's path-following performance relative to the unassisted case. According to Table IV, the maximum tracking error decreases from 2.5244 m in the unassisted configuration to 1.7456 m and 1.6111 m for the proposed fuzzy assist map and the saturated linear assist curve, respectively. Similar improvements are observed in the RMS tracking error, indicating that steering assistance becomes increasingly beneficial as the steering task becomes more demanding at higher vehicle speeds.

The driver torque responses presented in Fig. 15(b) demonstrate a substantial reduction in steering effort for both assist strategies. The proposed fuzzy assist map reduces the maximum and RMS driver torque by 54.16% and 51.54%, respectively, while the saturated linear assist curve achieves larger reductions of 63.28% and 61.34%. Although the linear assist curve provides the greatest reduction in driver effort, its higher assist level may diminish steering feel by excessively reducing the torque perceived by the driver. In contrast, the fuzzy assist map provides a more moderate level of assistance that remains sufficient to substantially reduce driver workload while preserving a more balanced interaction between the driver and the steering system.

The steering column angle responses shown in Fig. 15(c) remain comparable for all configurations, confirming that neither assist strategy alters the intended steering trajectory. More pronounced differences are observed in the steering column angular velocity response shown in Fig. 15(d). Rapid steering reversals generate transient angular-velocity peaks for both assist strategies; however, the saturated linear assist curve exhibits noticeably larger peaks and greater high-frequency oscillations. This observation is supported by the quantitative results in Table VI, where the maximum angular-velocity error reaches 92.93 deg/s for the linear assist curve compared with 63.30 deg/s for the proposed fuzzy assist map. Likewise, the RMS angular-velocity error is reduced from 18.87 deg/s to 15.44 deg/s. These results indicate that the fuzzy assist map provides a better-damped steering response with fewer abrupt dynamic variations while maintaining a high level of steering assistance.

Overall, both assist strategies improve tracking performance and substantially reduce driver workload compared with the unassisted configuration. However, the proposed fuzzy assist map achieves a more favorable balance between steering assistance, steering smoothness, and driver feedback by avoiding the excessive transient steering dynamics associated with the saturated linear assist curve while still providing significant reductions in steering effort.

c) Case III Low-speed Operation Under External Disturbance

The low-speed disturbance scenario evaluates the response of the steering system to the deterministic external disturbance defined by (22), which is applied as an equivalent disturbance torque at the steering column. As shown in Table V and Fig. 16(a), all three configurations maintain nearly identical path-tracking performance compared with the nominal low-speed case. The maximum and RMS tracking errors exhibit only negligible variations, indicating that the applied disturbance does not significantly affect the vehicle's ability to follow the reference trajectory.

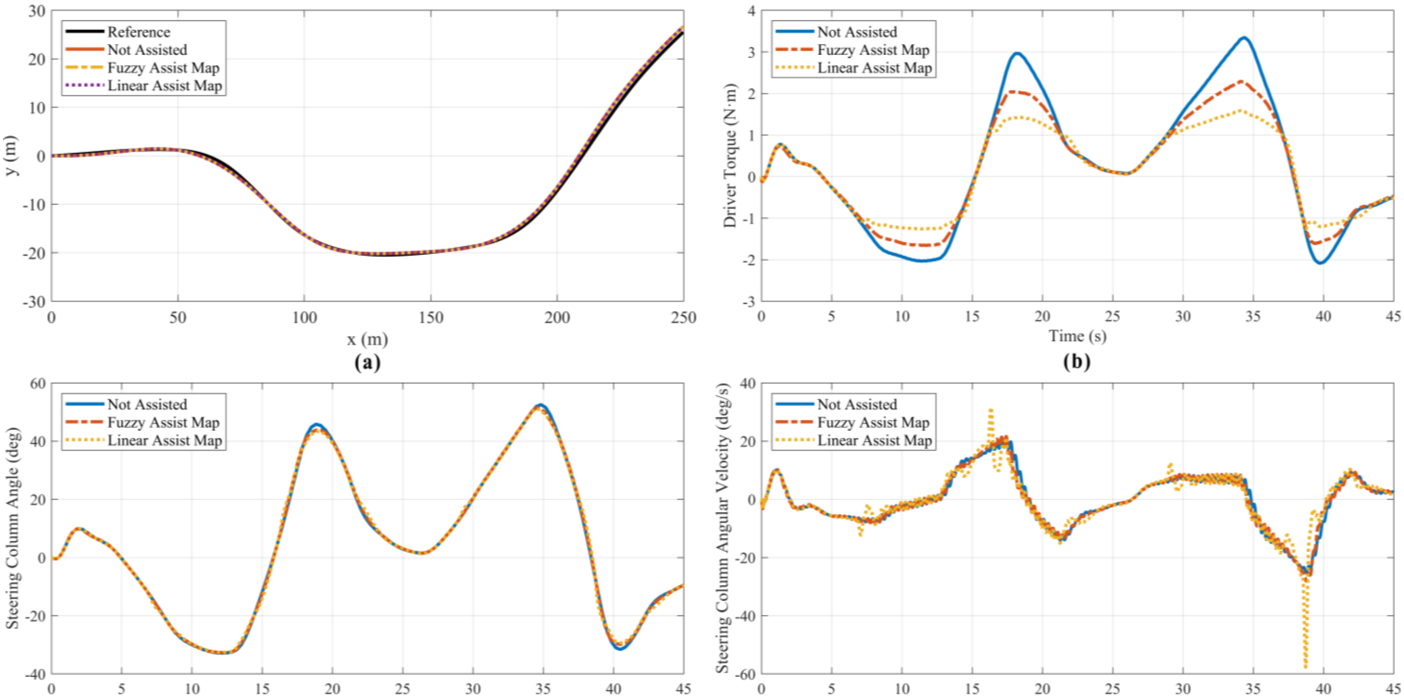

Fig. 15 ***(Case II. V=50 km/h)***. (a) path tracking performance (b) Driver torque demand (c) steering column angle (d) steering column angular velocity

The influence of the disturbance becomes more evident in the steering effort required from the driver, as shown in Fig. 16(b). The deterministic disturbance introduces small oscillatory variations into the driver torque signal. Both assist strategies continue to reduce the steering effort considerably; however, the saturated linear assist curve reacts more aggressively to the disturbance, producing larger torque fluctuations. In contrast, the proposed fuzzy assist map provides a smoother torque profile by continuously adapting the assistance level according to the steering conditions, thereby preventing unnecessary amplification of the disturbance-induced oscillations.

The differences between the assist strategies become more apparent in the steering column responses shown in Fig. 16(c) and Fig. 16(d). The steering column angle remains almost unchanged for all configurations, demonstrating that the disturbance does not alter the driver's intended steering command. However, the steering column angular velocity reveals a clear difference in dynamic behavior. Although both assist strategies follow the same overall steering motion, the saturated linear assist curve exhibits larger transient peaks and more noticeable oscillatory behavior. According to Table VII, the maximum steering-column angular velocity error reaches 32.59 deg/s for the saturated linear assist curve, compared with only 5.37 deg/s for the proposed fuzzy assist map. Likewise, the RMS angular velocity error is reduced from 3.36 deg/s to 1.11 deg/s, corresponding to a decrease in RMS error percentage from 13.26% to 4.39%. These results indicate that the fuzzy assist map effectively suppresses disturbance-induced steering oscillations while maintaining a smooth steering response.

The driver torque reduction results reported in Table V further demonstrate that both assist strategies retain their effectiveness under disturbance. The proposed fuzzy assist map achieves a 31.57% reduction in maximum driver torque, while the saturated linear assist curve achieves 52.56%. Compared with the nominal low-speed case, the reductions decrease only slightly because a portion of the assist motor torque is utilized to compensate for the applied disturbance in addition to reducing driver effort. The relatively small change confirms the satisfactory disturbance-rejection capability of both assist strategies.

Overall, the proposed fuzzy assist map preserves tracking accuracy and driver torque reduction while substantially reducing disturbance-induced oscillations in the steering system. Consequently, it provides smoother steering behavior and improved steering feel compared with the saturated linear assist curve.

d) Case IV. High-speed Operation Under External Disturbance

At 50 km/h, the steering system is subjected to higher steering demands while following the reference path. Although the disturbance defined by (22) is applied throughout the maneuver, its magnitude remains relatively small compared with the steering torques generated during high-speed operation. Consequently, its influence on the overall steering response is limited.

This behavior is reflected in Table V and Fig. 17(a), where the path-tracking performance remains very similar to that of the nominal high-speed case. Both assist strategies continue to provide noticeable improvements over the unassisted configuration. The maximum tracking error is reduced from 2.3283 m in the unassisted case to 1.6786 m and 1.5609 m for the fuzzy assist map and saturated linear assist curve, respectively. Similar improvements are observed in the RMS tracking error, confirming that the applied disturbance does not significantly degrade the vehicle's path-following capability.

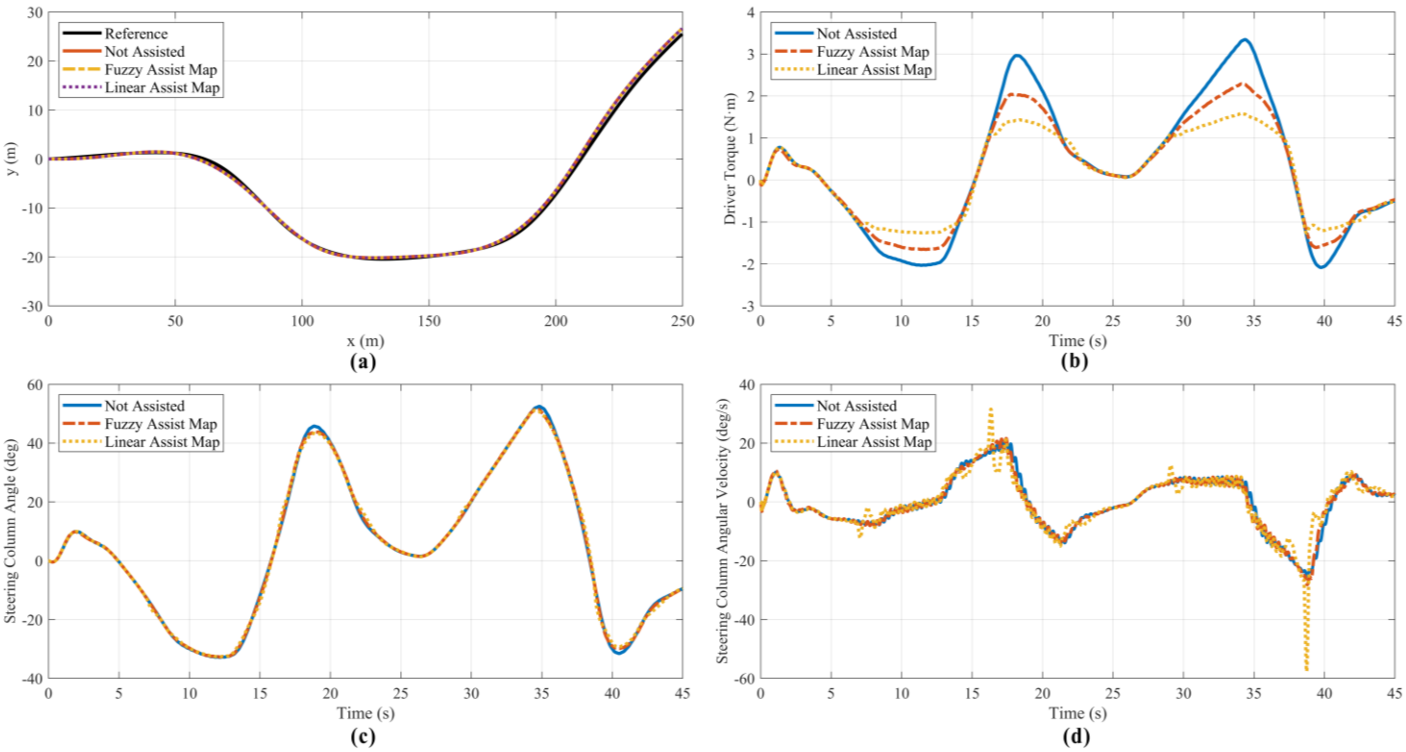

Fig. 16 ***(Case III. V=20 km/h, operating under disturbance)***. (a) path tracking performance (b) Driver torque demand (c) steering column angle (d) steering column angular velocity

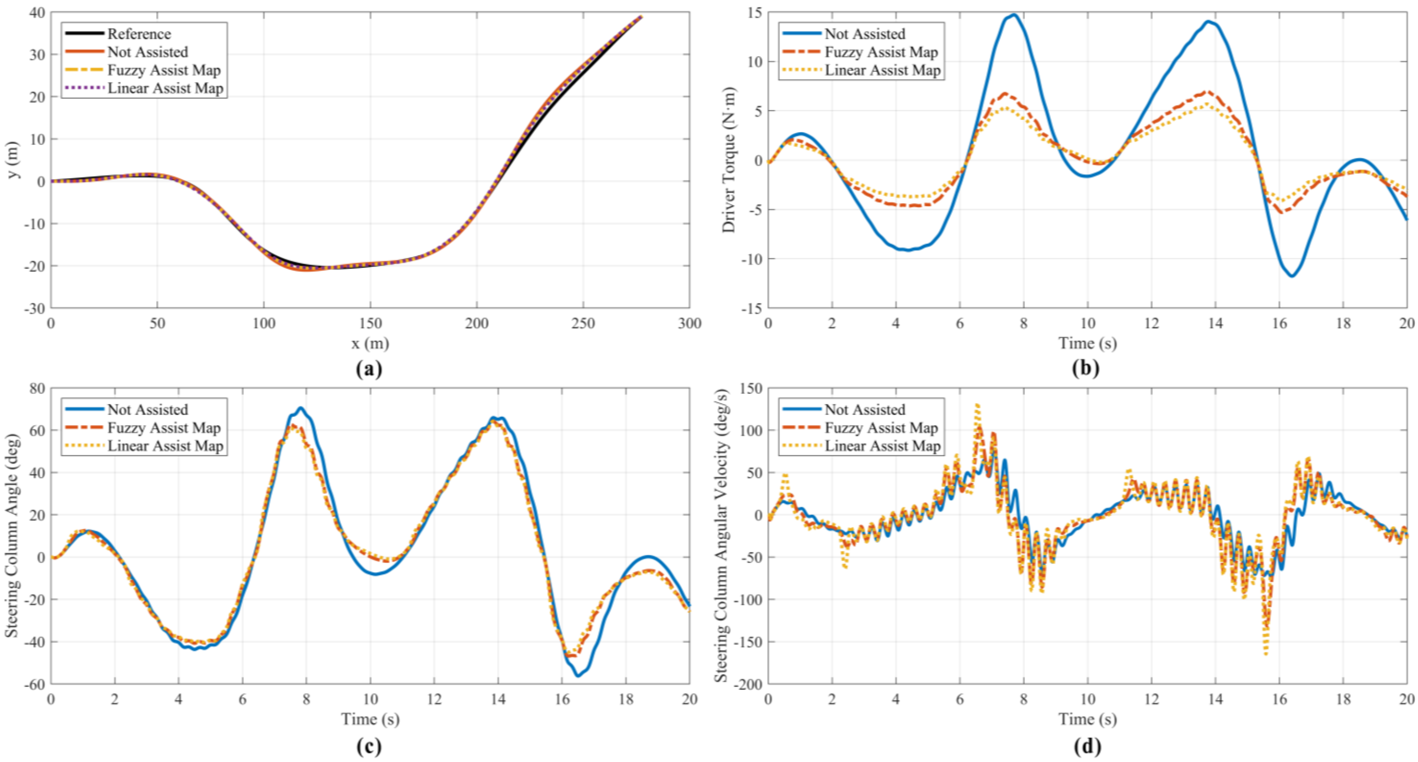

Fig. 17 ***Case IV. (V=50 km/h, operating under disturbance)***. (a) path tracking performance (b) Driver torque demand (c) steering column angle (d) steering column angular velocity

The driver torque responses shown in Fig. 17(b) demonstrate that both assist strategies continue to provide substantial reductions in steering effort under disturbed conditions. The proposed fuzzy assist map achieves a 52.57% reduction in maximum driver torque, while the saturated linear assist curve achieves 61.44%. Although both methods remain effective, the linear assist curve continues to exhibit a more aggressive assistance characteristic, whereas the fuzzy assist map provides smoother and more progressive torque support throughout the maneuver.

The differences between the assist strategies become more pronounced in the steering column responses shown in Fig. 17(c) and Fig. 17(d). The steering column angle remains nearly unchanged, indicating that neither assist strategy alters the intended steering command. However, the steering column angular velocity exhibits significant oscillatory behavior due to the applied disturbance. While both assist strategies experience disturbance-induced oscillations, the proposed fuzzy assist map maintains lower angular velocity errors throughout the maneuver. As reported in Table VII, the maximum steering-column angular velocity error is 63.81 deg/s for the fuzzy assist map compared with 95.21 deg/s for the saturated linear assist curve. Likewise, the RMS angular velocity error is reduced from 18.31 deg/s to 14.58 deg/s, corresponding to a decrease in RMS error percentage from 23.42% to 18.66%. These results indicate that the fuzzy assist map provides better damping of disturbance-induced steering oscillations while maintaining a stable steering response.

The torque reduction values presented in Table V decrease only slightly compared with the corresponding nominal high-speed case. Similar to Case III, part of the assist motor output is utilized to compensate for the applied disturbance in addition to reducing driver effort. Nevertheless, the reductions remain very close to those obtained under nominal conditions, demonstrating that both assist strategies preserve their steering assistance capability in the presence of external disturbance.

Overall, both assist strategies exhibit satisfactory disturbance-rejection performance during high-speed operation. However, the proposed fuzzy assist map provides a more balanced steering response by maintaining comparable tracking performance while reducing steering-column velocity errors and limiting disturbance-induced oscillations, thereby improving steering smoothness and driver comfort compared with the saturated linear assist curve.

Fig. 18 illustrates the motor energy consumption for all four test conditions, comparing the proposed fuzzy assist map with the saturated linear assist curve. Subplots (a) and (b) correspond to the low-speed (20 km/h) and high-speed (50 km/h) undisturbed cases, while (c) and (d) present the respective disturbance scenarios. Across all operating conditions, the fuzzy assist map consistently demonstrates superior energy efficiency, exhibiting noticeably lower cumulative energy consumption in every case.

The observed reduction in energy consumption cannot be attributed solely to the lower assist levels provided at higher vehicle speeds. From a physical standpoint, the power delivered by the EPS motor is proportional to the product of motor torque and steering column angular velocity. Therefore, the total energy consumption depends not only on the magnitude of the assist torque but also on the dynamic response of the steering system. While the adaptive characteristics of the fuzzy assist map reduce unnecessary assistance when high assist levels are not required, they also produce smoother torque transitions and more gradual steering responses.

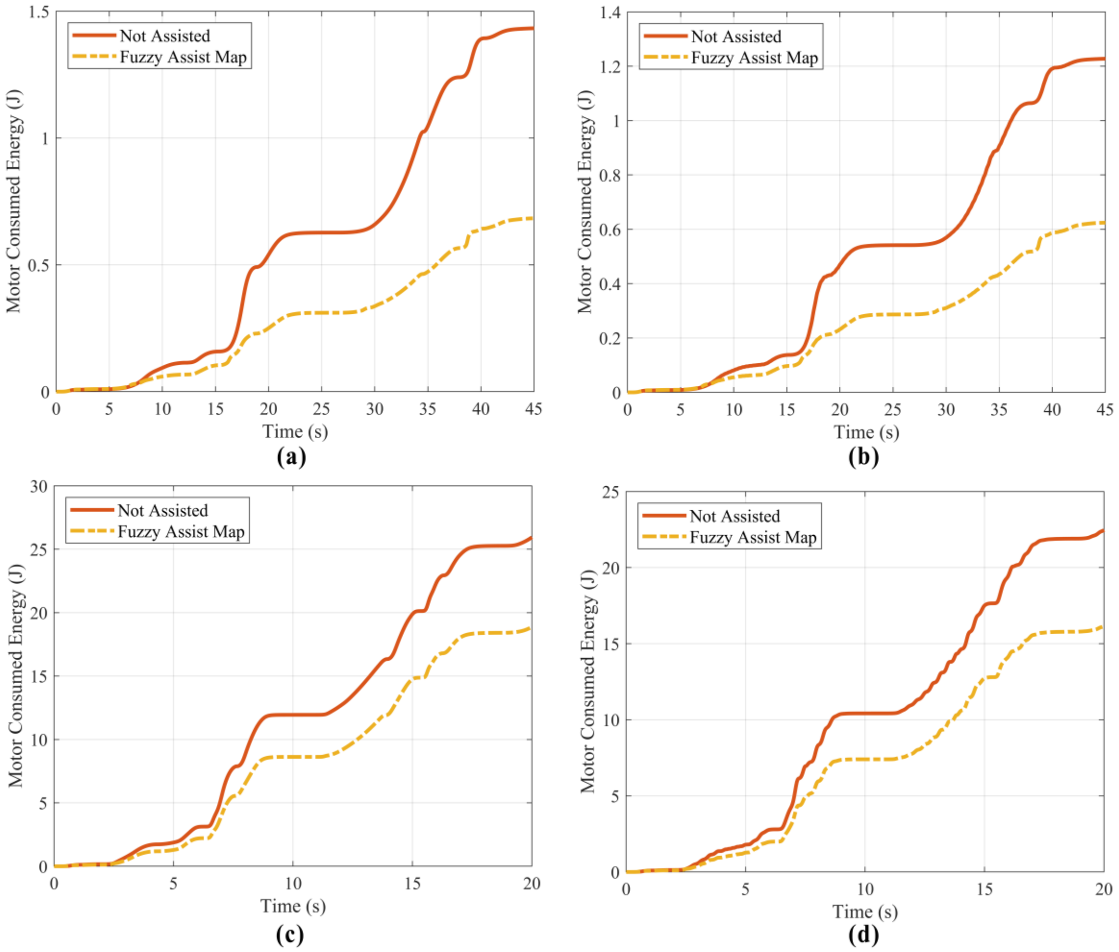

Fig. 18 Assist motor energy consumption across all four cases. (a) Case I (b) Case II (c) Case III (d) Case IV

In contrast, the saturated linear assist curve exhibits more aggressive torque variations and sharper transient responses, particularly during steering corrections and disturbance rejection. As observed in the steering-column angular velocity results, the linear assist strategy generates pronounced velocity spikes, especially at higher vehicle speeds. These rapid steering motions increase the instantaneous motor power demand even when the average assist torque remains comparable. Consequently, the higher energy consumption of the linear assist curve is caused not only by unnecessary torque generation near low driver-torque regions, but also by the increased angular velocity peaks and oscillatory behavior of the steering system. By providing smoother, context-aware assist torque and reducing abrupt steering-column motions, the fuzzy assist map lowers both the required assist torque and the associated power peaks. This results in reduced instantaneous power demand and lower cumulative motor energy consumption under both nominal and disturbed operating conditions.

TABLE IV COMPARATIVE TRACKING ERRORS AND TORQUE DEMAND REDUCTION FOR CASES I & II

Velocity	Assist mode	Max y error (m)	Max y error %	Rms y error (m)	Rms y error %	Max driver torque reduction %	Rms driver torque reduction %
V=20 km/h	Not Assisted	1.4131	3.07	0.5904	1.28		
	Fuzzy Assist map	1.3701	2.98	0.5845	1.27	33.65	22.68
	Saturated linear assist curve	1.3344	2.90	0.5809	1.26	54.30	39.61
V=50 km/h	Not Assisted	2.5244	4.24	0.9330	1.57		
	Fuzzy Assist map	1.7456	2.93	0.6952	1.17	54.16	51.54
	Saturated linear assist curve	1.6111	2.71	0.6573	1.11	63.28	61.34

TABLE V COMPARATIVE TRACKING ERRORS AND TORQUE DEMAND REDUCTION FOR CASES III & IV

Velocity	Assist mode	Max y error (m)	Max y error %	Rms y error (m)	Rms y error %	Max driver torque reduction %	Rms driver torque reduction %
V=20 km/h	Not Assisted	1.3992	3.04	0.5882	1.28		
	Fuzzy Assist map	1.3628	2.96	0.5833	1.27	31.57	20.90
	Saturated linear assist curve	1.3312	2.90	0.5802	1.26	52.56	37.06
V=50 km/h	Not Assisted	2.3283	3.91	0.8662	1.46		
	Fuzzy Assist map	1.6786	2.82	0.6756	1.14	52.57	49.99
	Saturated linear assist curve	1.5609	2.62	0.6436	1.08	61.44	59.88

TABLE VI STEERING COLUMN STATE METRICS FOR CASES I & II

Velocity	Assist mode	Max θ_c (deg)	Max $\dot{\theta}_c$ (deg/s)	Max θ_c error (deg)	Rms θ_c error (deg)	Rms θ_c error %	Max $\dot{\theta}_c$ error (deg/s)	Rms $\dot{\theta}_c$ error (deg/s)	Rms $\dot{\theta}_c$ error %
V=20 km/h	Fuzzy Assist map	51.524	28.029	2.2441	0.6276	1.20	5.6924	1.2751	5.19
	Saturated linear assist curve	51.123	59.768	4.1415	1.1750	2.24	35.3210	3.5923	14.63
V=50 km/h	Fuzzy Assist map	63.559	132.441	19.4456	6.3823	8.94	63.3002	15.4402	22.18
	Saturated linear assist curve	63.487	162.506	22.3462	7.3762	10.33	92.9322	18.8667	27.10

TABLE VII STEERING COLUMN STATE METRICS FOR CASES III & IV

Velocity	Assist mode	Max θ_c (deg)	Max $\dot{\theta}_c$ (deg/s)	Max θ_c error (deg)	Rms θ_c error (deg)	Rms θ_c error %	Max $\dot{\theta}_c$ error (deg/s)	Rms $\dot{\theta}_c$ error (deg/s)	Rms $\dot{\theta}_c$ error %
V=20 km/h	Fuzzy Assist map	51.5241	28.143	2.001	0.5394	1.03	5.3692	1.112	4.39
	Saturated linear assist curve	51.155	57.676	4.0803	1.0803	2.06	32.5861	3.3583	13.26
V=50 km/h	Fuzzy Assist map	64.273	131.295	16.8164	5.4448	7.72	63.8072	14.5841	18.66
	Saturated linear assist curve	64.102	164.534	19.5382	6.3201	8.96	95.2068	18.3069	23.42

VII. CONCLUSION

This work developed a comprehensive electric power steering (EPS) modeling and control framework that integrates a 2-DOF lateral-yaw vehicle model with a high-fidelity steering column dynamic model incorporating torsion-bar compliance, motor and wheel inertias, damping, nonlinear steering friction, and self-aligning torque feedback from the road. Coupled with a future-predictive driver steering model, the resulting formulation captures the essential closed-loop interactions between the driver, steering mechanics, assist motor, and vehicle motion with sufficient fidelity for controller design and evaluation.

The main contribution of this study is the development of a compact, computationally efficient Sugeno-type fuzzy assist-torque map, deliberately designed with a minimal rule base to preserve interpretability while enabling nonlinear, speed-dependent assist behavior. Despite its structural simplicity, the fuzzy assist map consistently outperformed the saturated linear assist curve commonly adopted in the literature. Across all simulation cases, including low- and high-speed operation both with and without external disturbances, the proposed strategy delivered lower path-tracking errors, reduced driver torque demand, and significantly smoother steering column angle and angular velocity responses. In contrast, the linear assist curve exhibited aggressive high-speed amplification, abrupt assist transitions, and greater sensitivity to disturbance-induced steering oscillations, as evidenced by the steering-column angular velocity responses under disturbance conditions.

The proposed fuzzy strategy also demonstrated a clear advantage in energy performance, consuming noticeably less motor energy across all operating conditions due to its adaptive torque modulation, smoother steering dynamics, and avoidance of unnecessary assistance in low driver-torque regions. These results demonstrate that the fuzzy assist map provides a more favorable balance between steering feel, disturbance rejection, stability, and energy efficiency than conventional assist-curve formulations.

Future work will focus on hardware-in-the-loop and full experimental validation of the proposed approach. Implementing the fuzzy assist map on an EPS test bench or an in-vehicle prototype will enable assessment of driver perception, energy behavior under realistic loading conditions, and interaction with nonlinear tire dynamics and road disturbances. Future studies will also investigate the robustness of the proposed assist strategy under variations in vehicle mass, tire-road friction coefficient, and other uncertain vehicle parameters representative of real-world driving conditions. In addition, extending the framework to adaptive or learning-based assist strategies and incorporating coupled longitudinal-lateral vehicle dynamics with variable-speed operation represent promising directions for further research.

Overall, the study demonstrates that integrating vehicle and steering column dynamics with a compact fuzzy assist-torque mapping yields a practical, stable, and energy-efficient EPS assist solution suitable for next-generation vehicle steering systems.

Acknowledgment

This research was supported by Pirouz Auto Parts Development Group – Toos Pump and Steering and the Office of Industry Relations at Ferdowsi University of Mashhad, Mashhad, Iran (Grant Numbers: 102967 and 102511). We express our sincere gratitude to Mr. Poorghasemi of the Pirouz Auto Parts Development Group for his support and thoughtful advice. Additionally, we extend our heartfelt appreciation to all members of the Center for Advanced Rehabilitation & Robotics Research (FUMCARE) for their invaluable support.

References

[1] Jörnsen Reimpell, H. Stoll, and J. W. Betzler, *The Automotive Chassis*. Butterworth-Heinemann, 2001.

[2] G. Genta and L. Morello, *The Automotive Chassis*. Springer Nature, 2019.

[3] R. Hartono, H. R. Cha and K. J. Shin, "Optimized PID Control for Enhanced Electric Power Steering System Performance," *2024 International Conference on Informatics Engineering, Science & Technology (INCITEST)*, Bandung, Indonesia, 2024, pp. 1-5, doi: 10.1109/INCITEST64888.2024.11121507.

[4] Li, Y.; Yang, Z.; Zhai, D.; He, J.; Fan, J. Study on Control Strategy of Electric Power Steering for Commercial Vehicle Based on Multi-Map. World Electr. Veh. J. 2023, 14, 33. https://doi.org/10.3390/wevj14020033

[5] V. T. Ha, "Improvement of Torque Control for an Assistant Electric Power Steering System using a Type-2 Fuzzy Logic Controller," *Engineering Technology & Applied Science Research*, vol. 14, no. 4, pp. 14825–14831, Aug. 2024, doi: https://doi.org/10.48084/etasr.7494.

[6] T. A. Nguyen and T. L. Nguyen, "Nonlinear active disturbance rejection mechanism based sliding mode control for enhancing electric power assisted steering performance," *PLoS ONE*, vol. 20, no. 4, pp. e0321664–e0321664, Apr. 2025, doi: https://doi.org/10.1371/journal.pone.0321664.

[7] M. Irmer and H. Henrichfreise, "Design of a robust LQG compensator for an electric power steering," IFAC-PapersOnLine, vol. 53, no. 2, pp. 6624–6630, 2020, doi: 10.1016/j.ifacol.2020.12.082.

[8] D. Fu, S. Rakheja, W.-B. Shangguan, and H. Yin, "Robust control for fuzzy electric power steering system: A two-layer performance approach," J. Vibrat. Control, vol. 28, nos. 5–6, pp. 536–550, Mar. 2022, doi: 10.1177/10775463211003420.

[9] Y. Li, T. Shim, D. Wang, and T. Offerle, "Model Reference Control-Based Steering Feel Improvement for Electric Power-Assisted Steering System," *Journal of Dynamic Systems, Measurement, and Control*, vol. 145, no. 4, Jan. 2023, doi: https://doi.org/10.1115/1.4056532.

[10] T. Chugh, F. Bruzelius, M. Klomp and B. Jacobson, "Steering Feedback Transparency Using Rack Force Observer," in *IEEE/ASME Transactions on Mechatronics*, vol. 27, no. 5, pp. 3853-3864, Oct. 2022, doi: 10.1109/TMECH.2022.3144245.

[11] B. Jang, D. Lee, K. Kim, and K.-S. Kim, "Road Torque Modeling for Electric Power Steering Systems," *International Journal of Automotive Technology*, vol. 23, no. 3, pp. 765–773, Jun. 2022.

[12] D. N. Nguyen and T. A. Nguyen, "Fuzzy backstepping control to enhance electric power steering system performance," IEEE Access, vol. 12, pp. 88681–88695, Jan. 2024.

[13] Z. Wang and H. R. Karimi, "Experimental study on antivibration control of electrical power steering systems," J. Appl. Math., vol. 2014, pp. 1–7, Jan. 2014.

[14] T. A. Nguyen, "Development of a novel integrated control strategy for automotive electric power steering systems," IEEE Trans. Autom. Sci. Eng., 2024.

[15] T. A. Nguyen, "Designing a new integrated control solution for electric power steering systems based on a combination of nonlinear techniques," PLoS One, vol. 19, no. 9, Sep. 2024.

[16] T. A. Nguyen and J. Iqbal, "Genetic algorithm inspired optimal integrated nonlinear control technique for an electric power steering system," J. Braz. Soc. Mech. Sci. Eng., vol. 46, no. 11, Oct. 2024.

[17] S. You, G. Kim, S. Lee, D. Shin, and W. Kim, "Neural approximation-based adaptive control using reinforced gain for steering wheel torque tracking of electric power steering system," IEEE Trans. Syst. Man Cybern. Syst., vol. 53, no. 7, pp. 4216–4225, Feb. 2023.

[18] H. Pang, G. Xu, Z. Song, D. Zhao, W. Wang, and P. Diao, "EPS system of tractor automatic driving: An improved LMI with mixed sensitivity control method," J. Electr. Comput. Eng., vol. 2021, Art. no. 2021, 2021.

[19] R.-O. Nemes, M. Ruba, and C. Martis, "Integration of real-time electric power steering system Matlab/Simulink model into National Instruments VeriStand environment," in 2022 IEEE 20th International Power Electronics and Motion Control Conference (PEMC), Aug. 2018, doi: https://doi.org/10.1109/epepemc.2018.8521888.

[20] T. A. Nguyen, "Proposing a novel nonlinear integrated control technique for an electric power steering system to improve automotive dynamic stability," Proc. Inst. Mech. Eng., Part K: J. Multi-body Dyn., 2024.

[21] Q. Liu, W. Kong, and T. Li, "The assist curve design for electric power steering system," in Proc. 2nd Int. Conf. Advances in Mechanical Engineering and Industrial Informatics, 2016.

[22] M. Allous, K. Mrabet, and N. Zanzouri, "Fast fault-tolerant control of electric power steering systems in the presence of actuator fault," Proc. Inst. Mech. Eng., Part D: J. Automobile Eng., vol. 233, no. 12, pp. 3088–3097, 2018.

[23] Y. Li, G. Wu, L. Wu, and S. Chen, "Electric power steering nonlinear problem based on proportional–integral–derivative parameter self-tuning of back propagation neural network," Proc. Inst. Mech. Eng., Part C: J. Mech. Eng. Sci., vol. 234, no. 23, pp. 4725–4736, 2020.

[24] T. Niu, "Measurement and modelling of human car driving with steering torque feedback," Ph.D. dissertation, Dept. of Eng., Univ. of Cambridge, Christ's College, Cambridge, UK, Sep. 2021.T.

[25] T. A. Nguyen and D. N. Nguyen, "An integrated SMC–NADRC robust control approach for electric power steering systems considering nonlinear friction and parametric uncertainties," PLOS ONE, vol. 21, no. 4, Art. no. e0346332, 2026, doi: 10.1371/journal.pone.0346332.

[26] M. A. Zakaria, H. Zamzuri, S. A. Mazlan, and S. M. H. F. Zainal, "Vehicle path tracking using future prediction steering control," *Procedia Eng.*, vol. 41, pp. 473–479, 2012.

[27] Z. Rezaee and M-R Akbarzadeh-T, "Uncertainty Management in the Dynamics of Biological Systems: A Key to Goal-oriented Rehabilitation," Basic and Clinical Neuroscience Journal, vol. 16, no.1, pp. 143–158, 2025.